THE JOURNAL OF PHYSICAL CHEMISTRY C

Article

Cite This: J. Phys. Chem. C 2019, 123, 15330−15338

pubs.acs.org/JPCC

Novel Metallic Clathrates of Group-IV Elements and Their Compounds in a Dense Hexagonal Lattice

Taylan Gorkan,[†] Ilkay Ozdemir,[†] M. Yagiz Bakir,[†] Fatih Ersan,[†] Gökhan Gökoğlu,[‡] Ethem Aktürk,*[,†,¶] and Salim Ciraci*[,§]

[†]Department of Physics and [¶]Nanotechnology Application and Research Center, Adnan Menderes University, 09100 Aydın, Turkey

[‡]Department of Mechatronics Engineering, Faculty of Engineering, Karabuk University, 78050 Karabuk, Turkey

[§]Department of Physics, Bilkent University, 06800 Ankara, Turkey

Supporting Information

ABSTRACT: Further, to recently introduced metallic $NaSi_6$ and Si_6 clathrate structures, we show that not only Si but also other group-IV elements, such as C, Ge, and Sn, can form stable and metallic clathrate structures with open channels at the corners of hexagons. These elemental clathrates of Si, Ge, and Sn can be viewed as if they are a combination of 2D metallic planes and perpendicular 1D metallic chains, the interplay of which can give rise to interesting physical effects. When free-standing, these atomic planes transform to 2D semiconducting, single-layer structures. The clathrate structure of C, which consists of weakly interacting, vertical hexagonal tubes situated at the corners of a 2D hexagonal lattice, is insulating in the plane but 1D metallic perpendicular to the planes. We also show that stable compound clathrate structures can form by hosting different alkali, alkaline earth, and light transition metal atoms in the open channels of elemental clathrates. These new metallic allotropes of group-IV elements predicted by first-principles calculations based on the density functional theory exhibit features that can be critical fundamentally and technologically.

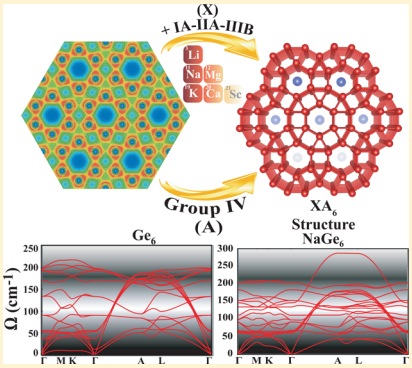

INTRODUCTION

Silicon (Si) is the most important, insofar as one of the most abundant group-IV elements on Earth. The cubic diamond (CD) structure, namely, the phase corresponding to the global minimum, has an open structure held by tetrahedrally coordinated covalent bonds constructed by sp^3-bond orbitals and high metallicity according to the scale of the bond-orbital model.[1−3] The fundamental band gap of 1.1 eV, excellent mechanical properties, and capacity to be grown into a large-size single crystal have made silicon in the CD structure the most crucial ingredient of modern microelectronics. The vision of using well-developed silicon technology in flexible 2D nanoelectronics has led to the prediction of stable Si single-layers, namely, silicene,[4,5] which was already grown on a Ag(111) substrate in single-layer and multilayer forms. Three-dimensional (3D) layered stable, eclipsed, and staggered structures of Si constructed by stacking trigonal and hexagonal dumbbell single-layers[6] named as silicite[7] appear to be a challenge at the experimental site. Besides, silicon can also be grown in the wurtzite structure and in various metastable forms such as amorphous, porous clathrates.

Semiconducting silicon in the CD structure can undergo a metal−insulator transition at high pressure, in extreme conditions realized in a diamond anvil cell. The transition follows the sequence Si-1 → Si-2 (β-Sn structure) at about 10 GPa → Si-11 (*Imma*-Si) → Si-5 (SH, simple hexagonal structure) at about 15 GPa → Si-6 (*Cmca*-Si) at about 38 GPa → Si-7 (hexagonal close-packed) at about 40 GPa → Si-10 (face-centered cubic) at about 80 GPa.[8−14]

Germanium, being another group-IV element just below Si, shows also a phase transition from a semiconducting CD structure to a β-Sn structure at 10 GPa, to *Imma* at 75 GPa, to SH at 85 GPa, to *Cmca* at 100 GPa, and to hcp at 170 GPa.[15] Although the sequence of the structural transitions of Ge is similar to Si, transition pressures are higher than Si due to 3d core states behind the 4s and 4p valence states.

However, due to strong kinetic effects, the structural transitions occurring at a high pressure are not completely reversible upon pressure release at ambient temperature. This causes various metastable phases to form through pressure release such as Si-12 (R8, rhombohedral) and Si-3 (BC8, body-centered).[13,16−18] Subsequent thermal annealing of BC8-Si results in Si-4 (hexagonal diamond) formation.[13,17] By rapid release of pressure from the metallic state, two metastable phases of Si with a tetragonal structure, referred as Si-8 and Si-9, have been discovered.[19] Other metastable phases with a tetragonal structure of Si, BT8 and ST12, have been produced by Rapp et al. by microexplosion experiments and computa-

Received: April 8, 2019
Revised: May 10, 2019
Published: May 22, 2019

ACS Publications © 2019 American Chemical Society

DOI: 10.1021/acs.jpcc.9b03270
J. Phys. Chem. C 2019, 123, 15330−15338

tional research within ab initio calculations.[20] They have reported that these new phases are likely to exhibit interesting properties, such as predicted narrow band gap semiconductor (BT8-Si) and potentially superconducting behavior (ST12-Si).

Numerous studies on the synthesis of other Si allotropes by using appropriate chemical precursors followed by physical and chemical manipulations have been published.[9,10,13,17,19−27] However, up until the study of Sung et al.,[28] the reported metastable Si allotropes were semiconducting; pure metallic Si phases at ambient conditions have not been investigated yet. Sung et al.[28] reported the prediction of pure metallic Si allotropes with open channels at ambient pressure and named it P6/m-Si_6. They show that this metallic phase can be obtained by removing Na after pressure release from a novel Na-Si clathrate called P6/m-$NaSi_6$. To examine low-enthalpy Na-Si allotropes with various composition ratios, they utilized an ab initio evolutionary crystal structure search method that combines conformational space annealing algorithm[29] for global optimization and first-principles electronic structure calculations. Furthermore, they have confirmed that both P6/m-$NaSi_6$ and P6/m-Si_6 are stable and can be superconductors with the critical temperatures of about 13 and 12 K at zero pressure, respectively. It is estimated that all of these metastable Si allotropes exhibit a wide range of features not only scientifically but also technologically. Moreover, the success in the exploration of new Si phases raises the question of whether other similar materials can form.

In this study, we investigated clathrates of group-IV elements, namely, P6/m-A_6 (or shortly A_6) and P6/m-XA_6 compounds (or XA_6) (with A = C, Si, Ge, and Sn; alkali metal atoms X = Li, Na, K; alkaline earth metal atoms X = Mg, Ca, Be; 3d transition metal atoms X = Sc, Ti), based on first-principles density functional theory (DFT). Revealing clathrates beyond Si and Na-Si, increasing their density of states at the Fermi level, $D(E_F)$, with divalent atoms, and attaining magnetic properties with transition metal atoms have been the prime motivations for considering so many atoms. The stability of all clathrates, P6/m-A_6 and P6/m-XA_6, have been examined first based on dynamical and thermal stability analyses. Then, the structural parameters and cohesive energy of the stable structures have been calculated; their energy band structures and the character of bonds between the two nearest group-IV atoms and the metallic binding have been analyzed. With the hope of monitoring the density of states at the Fermi level and, hence, the transition temperature from normal to superconducting state T_c, the response of the P6/m-Si_6 structure to the applied biaxial compressive and tensile strain has been examined. Finally, the stability of a two-dimensional (2D) single-layer to be cleaved from the P6/m-Si_6 crystal, which has an atomic structure similar to ω-borophene,[30] has been investigated. The important and original findings of our paper are summarized as follows: (i) P6/m-A_6 (A = C, Ge, Sn) structures are dynamically and thermally stable at low and elevated temperatures. All of these structures are metallic with remarkable electronic density of states at E_F. (ii) The optimized P6/m-C_6 (or C_6) structure is composed of tubes of hexagons, which are brought together by weak van der Waals interaction. The system behaves as conducting hexagonal rods perpendicular to the *xy* plane, indicating one-dimensional (1D) conduction. The wide electronic barriers between hexagonal tubes hinder conduction in the *xy* plane. (iii) A_6 (A = Si, Ge, Sn) clathrates also form 1D metallic chains along the *z-axes*. However, Si_6, Ge_6, and Sn_6 permit 1D−2D conduction mixed in a 3D lattice. (iv) Both tensile and compressive strains in Si_6 decrease DOS at E_F, yielding lower electronic conduction. (v) We found that alkali, alkaline earth, and transition metals including 16 P6/m-XA_6 clathrate systems are both dynamically and thermally stable. These systems also depict metallic behavior.

COMPUTATIONAL DETAILS

We have performed first-principles calculations for total energy and electronic structure within DFT by using the plane-wave basis set and projector augmented-wave (PAW) potentials[31] as implemented in the Vienna ab initio simulation package (VASP).[32,33] The exchange-correlation potential is approximated with generalized gradient approximation (GGA) using Perdew−Burke−Ernzerhof (PBE) exchange correlation functional[34] including van der Waals (vdW) correction.[35] We have considered $2s^12p^0$, $3s^13p^0$, and $3s^13p^64s^1$ configurations for Li, Na, and K, respectively; $2s^22p^0$, $3s^23p^0$, and $3s^23p^64s^2$ for Be, Mg, and Ca, respectively; $2s^22p^2$, $3s^23p^2$, $4s^24p^2$, and $5s^25p^2$ for C, Si, Ge, and Sn, respectively; $3p^64s^23d^1$ for Sc; and $4s^23d^2$ for Ti as valence electrons. By using the conjugate-gradient algorithm,[36,37] all the atomic positions and lattice parameters are fully optimized until the forces on each atom are less than 1.0×10^{-4} eV/Å. The convergence criterion of self-consistent calculations is taken to be 10^{-5} eV for total energy values. Pressures on the lattice unit cell are reduced to values less than 0.5 kB. The partial occupancies are determined using the Methfessel−Paxton scheme[38] with the smearing width of 0.2 eV. For the Brillouin zone (BZ) integration in the **k**-space, a set of $(15 \times 15 \times 30)$ **k**-point sampling is used within the Monkhorst−Pack scheme.[39] For the charge-transfer analysis, the effective charge on atoms is obtained using the Bader method.[40] The cohesive energy of an elemental clathrate (per atom), $E_c[A_6]$, is calculated using the expression $E_c[A_6] = (6E_T[A] - E_T[A_6])/n$, with $n = 6$. Similarly, the average cohesive energy of a compound clathrate is $E_c[XA_6] = (E_T[X] + 6E_T[A] - E_T[XA_6])/n$. Here, $E_T[A_6]$, $E_T[XA_6]$, $E_T[A]$, and $E_T[X]$, respectively, are the total energies of the elemental clathrate, compound clathrate, free A atom, and free X atom. n is the number of atoms in a unit cell. The formation energy (per atom), E_f, of an elemental clathrate A_6 is obtained by subtracting the cohesive energy of its counterpart in the CD structure corresponding to a global minimum from, that is, $E_f = E_c[A_6] - E_c[CD - A]$.

Phonon dispersion spectra are computed using force constants of the supercell within the framework of density-functional perturbation theory (DFPT),[41] as implemented in the VASP code combined with PHONOPY package.[42] In phonon calculations, an improved energy convergence criterion as 10^{-8} eV is attained to obtain well-converged real-space force constants. These calculations were performed using $2 \times 2 \times 2$ supercells. We have also carried out the thermal stability analysis of the systems by performing ab initio molecular dynamics (AIMD) simulations at 300, 500, and 1000 K. All the structures are visualized using the VESTA code.[43]

METALLIC 3D P6/M-A_6 ALLOTROPES OF GROUP-IV ELEMENTS

The P6/m clathrate structure has a simple 3D hexagonal lattice, allowing open channels to host suitable X metal atoms between adjacent hexagonal rings in the *xy*-plane. Group-IV

DOI: 10.1021/acs.jpcc.9b03270
J. Phys. Chem. C 2019, 123, 15330−15338

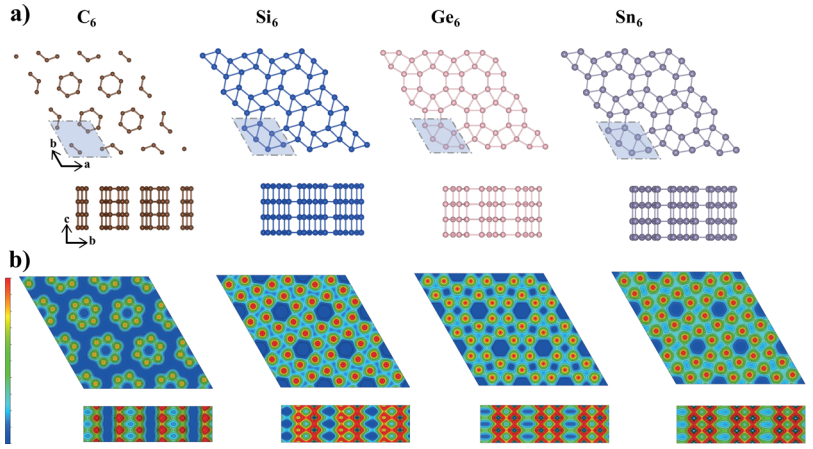

Figure 1. (a) Top (*xy* plane) and side views of the optimized atomic structure of the clathrate structures of group-IV elements P6/m-A_6 (or simply A_6) with A = C, Si, Ge, and Sn. Hexagonal primitive unit cells are shaded. (b) Contour plots of the total charge density at the lateral *xy*-plane passing through the hexagons and at the vertical plane. The color scale at the left side indicates shift from high density (red) to low density (dark blue). Open channels are shown as dark blue spots, and 1D conducting chains of atoms are shown as red/orange ribbons.

atoms, that is, A atoms, have five neighbors in the *xy*-plane and two neighbors in the adjacent atomic planes just below and above. This system is composed of 7-fold coordinated A atoms connected to seven neighboring A atoms with A−A bonds with slightly differing bond lengths. On the other hand, these A−A bonds are longer than the counterparts in the CD structure. In a recent work of Sung et al.,[28] it was reported that the P6/m-$NaSi_6$ clathrate structure can be synthesized at high pressure (12.4 GPa) conditions and the stability is preserved down to ambient pressure. Moreover, the pure P6/m-Si_6 system can be obtained by removing Na atoms from channels via thermal degassing. In the literature, this was the first metallic Si system that can be stabilized at ambient pressure. In the present work, we examine the clathrates of group-IV elements (A = C, Ge, Sn) in the P6/m structure. We included Si for the sake of comparison. The structures of the elemental (or bare) clathrates A_6 (A = C, Si, Ge, and Sn) are described in Figure 1a.

Structure Optimization and Stability. The calculated structural parameters as well as cohesive and formation energies of the elemental clathrates are presented in Table 1, together with those calculated for the counterparts in the CD structure. Our results related with the compound clathrates XA_6 will be presented in the forthcoming sections.

All A_6 crystals have positive cohesive energy, indicating that they are favorable energetically relative to their free atom constituents. This however does not ensure that these structures are structurally stable. Later, we will demonstrate their stability by the dynamical and thermal stability analyses. Normally, the cohesive energy of a clathrate A_6 is smaller than that of the counterpart in the CD structure in the global minimum. The difference is high in C_6 clathrate. Consistent with this conclusion, the calculated formation energies of C_6, Si_6, and Ge_6 are negative. Notably, E_f of Sn_6 is slightly positive. As for the A−A distances, they are significantly larger than the covalent bond lengths of the counterparts in the CD structure. For example, the Si−Si distances of Si_6 ranging between 2.48 and 2.62 Å are larger than the covalent bond of Si in the CD structure calculated as d = 2.34 Å.

Even if one starts from an initial clathrate structure P6/m-C_6 for C such as Si_6 clathrate, the structure has changed to the clathrate structure shown in Figure 1a upon optimization. This

Table 1. Values Calculated by Using PBE for P6/m-A_6 (A = C, Si, Ge, and Sn) and Their Counterparts in Cubic Diamond (CD) Structures[a]

	lattice constants				
structure	a (Å)	c (Å)	min. distance d (Å)	cohesive energy E_c (eV/atom)	formation energy E_f (eV/atom)
C_6	5.80	1.61	2.25	6.03	−1.91
Si_6	6.74	2.49	2.48	4.50	−0.33
Ge_6	7.27	2.65	2.62	3.85	−0.21
Sn_6	8.25	2.99	2.99	3.37	0.02
CD-C	3.56		1.54	7.94	
CD-Si	5.41		2.34	4.83	
CD-Ge	5.66		2.45	4.06	
CD-Sn	6.46		2.81	3.35	

[a]Lattice constants, |a| = |b| = a and |c| = c; minimum A−A distance, d; cohesive energy, E_c; formation energy, E_f.

structure is constructed from the tubes of hexagons, the centers of which are placed at the corners of the 2D hexagonal lattice. Nonetheless, it has a hexagonal lattice with a primitive unit cell containing six C atoms. The C−C distance between the atomic planes, namely, c, is 40% shorter than the in-plane C−C bonds. In this respect, the C_6 structure does not depict a layered character. On the other hand, the C−C bonds constructing hexagonal rings in the *xy* plane form strong bonds with a length comparable to that of graphene. Therefore, in the top view, C_6 appears as if it is graphene made of disconnected hexagons. The charge density isosurfaces depict the tubular character, with a very low charge density inside and around hexagonal tubes. Accordingly, it is expected that the hexagonal tubes are brought together by weak van der Waals interaction to form a C_6 structure. Such a situation occurs in 3D trigonal selenium and tellurium, where weakly interacting chiral tubes along the z direction are located also at the corners of a 2D hexagonal lattice.

Starting first from P6/m-Si_6, the lattice constants calculated in the present study, a = 6.74 Å and c = 2.49 Å, are in agreement with those calculated in ref 28. The cohesive energy of Si_6 is calculated as E_c = 4.50 eV per atom, comparable to that of the CD counterpart, which is calculated as 4.83 eV

DOI: 10.1021/acs.jpcc.9b03270
J. Phys. Chem. C 2019, 123, 15330−15338

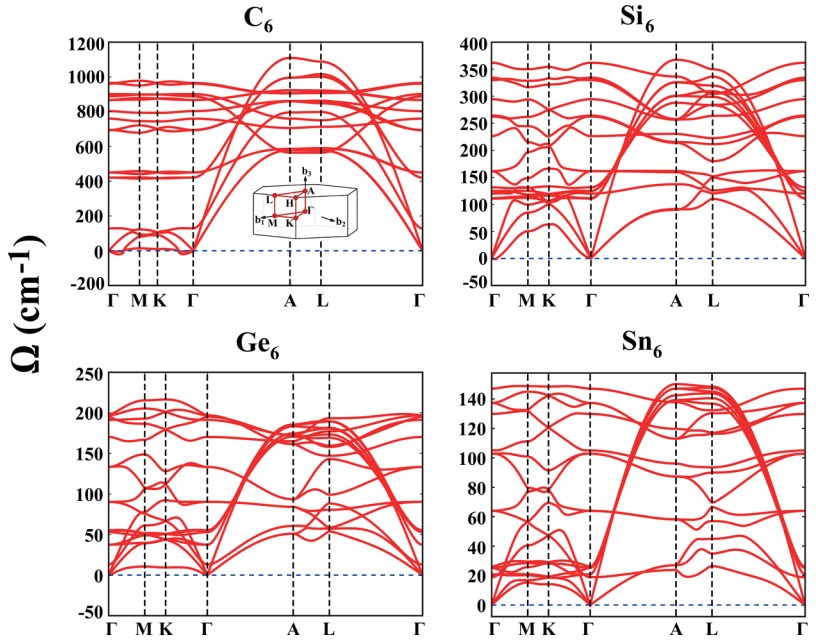

Figure 2. Phonon dispersion curves, that is, $\Omega(\mathbf{k})$, along major symmetry directions of the Brillouin zone calculated for the optimized structures of C_6, Si_6, Ge_6, and Sn_6. The Brillouin zone is described in the inset.

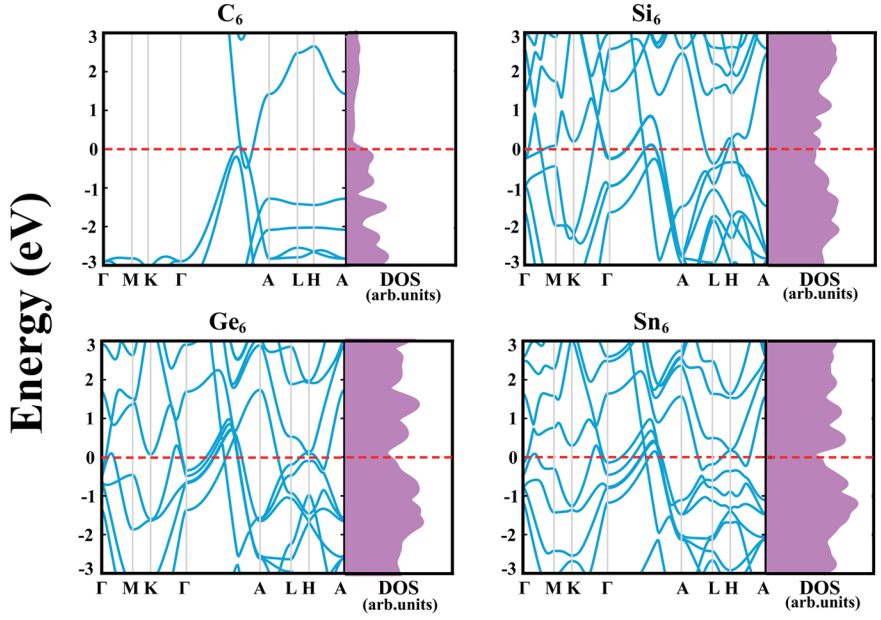

Figure 3. Electronic energy band structure $E_n(\mathbf{k})$ along major symmetry directions of the Brillouin zone and corresponding density of states (DOS) calculated for C_6, Si_6, Ge_6, and Sn_6. The zero of energy is set at the Fermi level and is shown by dashed lines.

(4.63 eV/atom determined experimentally). Table 1 and Figure 1a show that Ge_6 and Sn_6 clathrate structures display trends that are similar to those of Si_6. Charge density contour plots indicate that Si_6, Ge_6, and Sn_6 clathrates are rather different from C_6: all group-IV clathrates form metallic 1D vertical chains along the z axis, whereas the electronic charges of Si_6, Ge_6, and Sn_6 are delocalized in the xy atomic planes as a result of 5-fold coordination and constitute metallic bonding. Conversely, the charge of C_6 in the xy atomic planes of hexagons is localized between the C−C bonds of the hexagons. The implications of this distribution will be discussed in the forthcoming sections.

The dynamical stability of the elemental clathrates A_6 has been tested by the calculation of the frequencies of vibration modes. The eigenvalues of dynamical matrix, namely, the square of specific frequencies, $\Omega(\mathbf{k})^2$, would be negative in the absence of sufficient restoring force and hence could not return to its initial equilibrium position. At the end, the initial structure would be transformed to a different structure. Here, the calculated phonon dispersion curves of all A_6 clathrate structures presented in Figure 2 have positive frequencies along the symmetry axis of BZ. Only near the center of BZ, namely, $\lambda \rightarrow \infty$, specific modes can get imaginary values, which is well known to be an artifact of the numerical calculations. Notably, the phonon dispersion curves calculated

DOI: 10.1021/acs.jpcc.9b03270
J. Phys. Chem. C 2019, 123, 15330−15338

for Si_6 are in agreement with those calculated by Sung et al.[28] The dimensionality is well recognized in the phonon dispersions: While in-plane atoms have significant dispersion for the $\mathbf{k}\|xy$-plane, their dispersion is not high along the z axis. On the other hand, the optical modes, which are rather flat dispersion along Γ−M−K−Γ directions, attain high dispersion along the Γ−A direction, which is related with the metallic chain atoms along the z direction. These atoms display also a longitudinal branch with high dispersion along the Γ−A direction.

We also performed crude thermal stability analysis, which verifies that the elemental clathrate structures resist to thermal excitations at a high temperature. Based on this stability analysis, we concluded that the clathrate structures of group-IV elements keep their structural stability above the room temperature.

Electronic Energy Structure. The electronic band structures of the optimized A_6 clathrate structures and the densities of states are presented in Figure 3. The clathrate structures of four elements are metallic with several bands crossing the Fermi level. Because of the atomic configuration of C_6, which is rather different from Si_6, Ge_6, and Sn_6, its metallic bands depict dramatic differences. C_6 consists of weakly interacting hexagonal tubular structures, and the valence and conduction bands of the $\mathbf{k} \parallel xy$ plane (corresponding to Γ−M−K−Γ or A−L−H directions in BZ) are flat with a wide band gap between them. However, along the z direction, that is, the $\mathbf{k} \perp xy$-plane (corresponding to the Γ−A direction), energy bands are parabolic and cross the Fermi level. Under these circumstances, C_6 can be viewed as if it is a bundle of conducting hexagonal rods or tubes perpendicular to the xy atomic plane with a wide barrier between them that hinders the lateral conduction. Parabolic metallic bands of Si_6, Ge_6, and Sn_6 derived from vertical atomic chains can also be deduced along the Γ−A direction. Additionally, bands of the $\mathbf{k} \parallel xy$-plane (along Γ−M−K−Γ or A−L−H directions) also cross the Fermi level and contribute to the metallicity of these clathrate structures. Consequently, the density of states at the Fermi level, $D(E_F)$, is high. In view of these arguments, one can expect that C_6 is essentially a 1D conductor, but Si_6, Ge_6, and Sn_6 display a 2D and 1D conduction mixed in a 3D crystal. We therefore expect that these directional conductivity can reflect to other measurable properties, such as thermal conductivity, etc.

Effect of Biaxial Strain. Since Si_6 clathrates are open structures depicting a layered behavior, we examined the tunability of their electronic structure by biaxial strain ϵ. To this end, we considered a four-layer slab of Si_6 under a uniform biaxial strain and calculated the total energy $E_T(\epsilon)$ and the interlayer spacing c for a given compressive or tensile strain values. The variation of E_T with ε is given in Figure 4.

The response of E_T to the applied strain is significant; $E_T(\epsilon)$ is symmetric with respect to the direction (sign) of small ϵ, but asymmetric behavior appears for $|\epsilon| > 0.03$. The variation of $c(\varepsilon)$ is not monotonic. c decreases with increasing tensile strain $0.0 < \epsilon < 0.03$ linearly, but it increases with increasing compressive strain with a decreasing rate. Here, with the premise of modulating the superconducting transition temperature T_c, we calculated the density of states at the Fermi level, $D(E_F)$, of Si_6 corresponding to its optimized structure elastically deformed under strain, $|\varepsilon| = 0.0-0.05$. Densities of states (DOSs) calculated self-consistently in the energy range of -0.5 eV $< E <$ 0.5 eV are shown in Figure 4a,b. It is seen

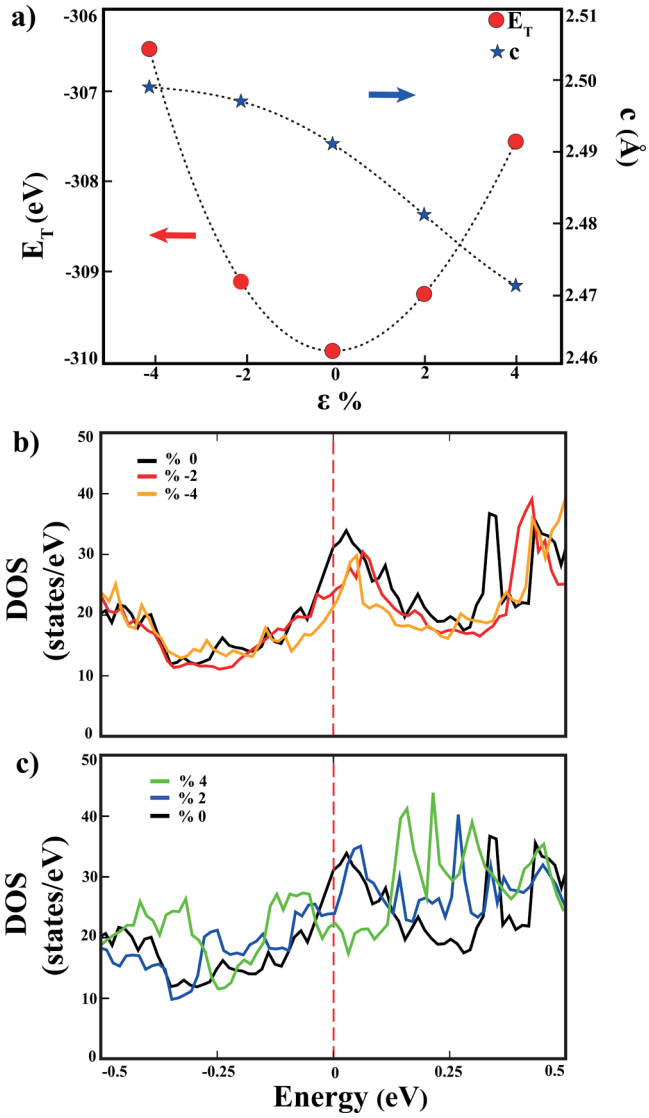

Figure 4. (a) Variation of the total energy E_T and interlayer spacing c with applied biaxial strain. (b) Variation of the density of states (DOS) near the Fermi level, $D(E_F)$, with the compressive biaxial strain. (c) Variation of the density of states near the Fermi level with the tensile biaxial strain. The zero of energy is set at the Fermi level.

that $D(E_F)$ decreases for both increasing tensile and compressive strains. Hence, no matter what is the type of biaxial strain, let it be tensile or compressive, the transition temperature T_c, electrical conductivity σ, and thermal conductivity κ of Si_6 shall decrease with increasing ϵ. This is a surprising, insofar an interesting result, and seems to be a complex interplay between the 1D/2D metallicity coexisting in Si_6 and reverse shifts of bands relative to the Fermi level thereof. For example, increasing 1D metallicity is compensated by decreasing 2D metallicity under the tensile strain.

Stability of Free-Standing Single-Layer of Si_6. The atomic plane of Si_6, as depicted by the top view in Figure 1, is similar to the structure of free-standing ω-borophene.[30] We further explored the question of whether a similar 2D free-standing single-layer can exist also for Si_6. Notably, silicene, that is, a single layer of silicon in a buckled honeycomb structure with electrons showing massless Dirac fermion behavior and ambipolar properties, was predicted earlier to be stable.[4,5] Later, silicene was synthesized on the Ag(111)

DOI: 10.1021/acs.jpcc.9b03270
J. Phys. Chem. C 2019, 123, 15330−15338

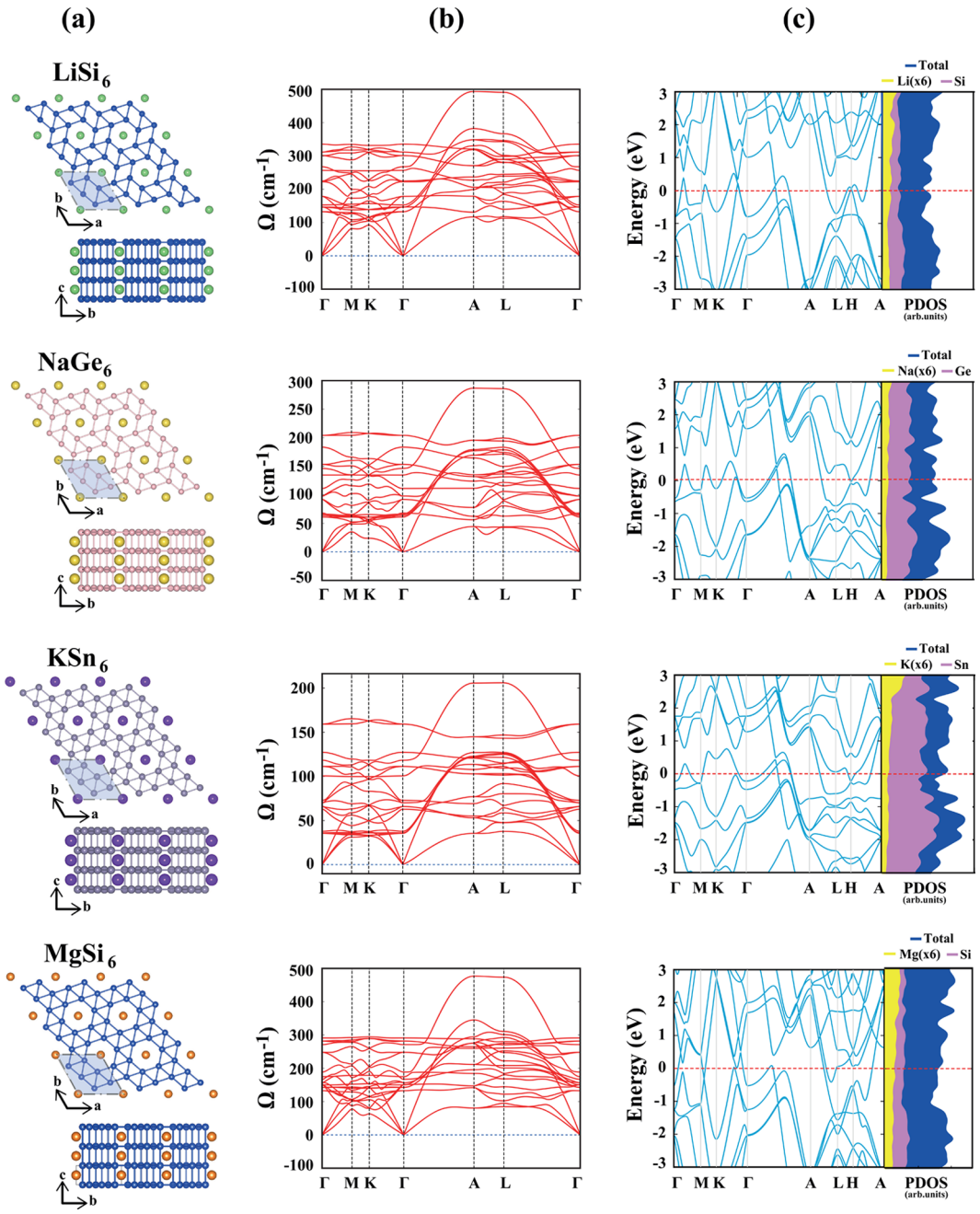

Figure 5. From left to right: (a) Top (*xy* plane) and side views of the optimized atomic configurations of compound clathrate structures of group-IV elements XA_6 with X = Li, Na, K, Mg and A = Si, Ge, Sn. Hexagonal primitive unit cells are shaded. (b) Corresponding phonon dispersion curves, $\Omega(\mathbf{k})$, calculated for the major directions of BZ. (c) Corresponding electronic energy band structure $E_n(\mathbf{k})$ and the total and atom-projected densities of states. The zero of energy is set at the Fermi level and is shown by dashed lines.

substrate.[44] Here, we optimized the atomic structure of a free-standing single-layer of nested hexagons. Interestingly, this planar single-layer underwent a structural transformation, whereby Si atoms formed a 2D structure consisting of deformed squares, hexagons, and octagons with 4- and 3-fold coordinated Si atoms having cohesion even stronger than that in silicene. Surprisingly, not only Si, but also Ge, compounds such as GaAs were shown to have a stable structure similar to Si. This surprising outcome of this study will be published elsewhere.

3D P6/M-XA_6 ALLOTROPES

Motivated with the earlier prediction of the P6/m-$NaSi_6$ (simply $NaSi_6$) clathrate structure,[28] we explored other possible compound clathrate structures XA_6 (A = C, Si, Ge, and Sn) and alkali, alkali earth, and 3d transition metal atoms (X = Li, Na, K, Mg, Ca, Be, Sc, Ti) to acquire different properties. The stability of all these structures was analyzed by calculating the frequencies of vibration modes, as described in the previous sections. Based on this analysis, XC_6 structures (X = Li, Na, and K) as well as XA_6 structures (X = Be and Ti; A = C, Si, Ge, Sn) had imaginary frequencies in BZ and were found to be unstable. The remaining 16 XA_6 metallic structures are

DOI: 10.1021/acs.jpcc.9b03270
J. Phys. Chem. C 2019, 123, 15330−15338

found to be stable based on the dynamical and thermal stability analyses. In Figure 5, we show optimized atomic structures, calculated phonon dispersion curves, and electronic energy band structures of the four selected clathrates. The optimized atomic structures and phonon dispersion curves of all stable XA_6 structures treated in this paper are presented in the Supporting Information. The calculated values of lattice constants and minimum distances between A−A and X−A atoms, cohesive energy, and effective charge on X atoms are presented in Table 2 for the 16 stable clathrate systems.

Table 2. Values Calculated by Using PBE for Stable P6/m-XA_6 (or Simply XA_6) Clathrate Structures for X = Li, Na, K, Ca, Mg, Sc and A = Si, Ge, Sn[a]

	lattice constant		min. distance			
structure	a (Å)	c (Å)	d_1 (Å)	d_2 (Å)	cohesive energy E_c (eV/atom)	charge transfer $\Delta\rho$ (e^-)
$LiSi_6$	6.79	2.49	2.51	2.80	4.33	−0.82
$NaSi_6$	6.99	2.52	2.56	2.98	4.18	−0.72
KSi_6	7.34	2.54	2.53	3.22	4.32	−0.63
$LiGe_6$	7.31	2.66	2.60	2.92	3.70	−0.82
$NaGe_6$	7.42	2.67	2.79	3.09	3.65	−0.72
KGe_6	7.74	2.72	2.73	3.35	3.53	−0.66
$LiSn_6$	8.29	2.97	2.96	3.31	3.50	−0.84
$NaSn_6$	8.33	3.00	3.02	3.37	3.47	−0.72
KSn_6	8.48	3.06	3.15	3.25	3.42	−0.66
$MgSi_6$	6.94	2.56	2.58	2.93	4.18	−1.44
$CaSi_6$	7.03	2.64	2.51	3.04	4.32	−1.13
$MgGe_6$	7.46	2.72	2.78	3.10	3.65	−1.24
$CaGe_6$	7.50	2.80	2.71	3.21	3.82	−1.16
$MgSn_6$	8.39	3.01	3.02	3.37	3.28	−1.07
$CaSn_6$	8.37	3.09	3.10	3.47	3.48	−1.17
$ScSi_6$	6.79	2.63	2.53	2.89	4.78	−1.09

[a]Lattice constants in the xy-plane, $|\mathbf{a}| = |\mathbf{b}| = a$; along the z -axis, $|\mathbf{c}| = c$; minimum distance between two neighboring A atoms, d_1; minimum distance between the neighboring X−A atoms, d_2; average cohesive energy per atom, E_c; the electronic charge transfer from the X (metal) atom to the A (group-IV) atom, $\Delta\rho$.

It is seen in Figure 5b that the inclusion of a guest alkali metal atom changes the overall vibrational spectra remarkably. A high-frequency optical mode, which is highly dispersive along the Γ−A−L−Γ directions, is distinguished in all clathrate systems caused by an alkali metal atom. This mode is not distinguishable only in $NaSi_6$ due to the small atomic mass difference of Na and Si atoms. Vibrational frequency range shifts to lower values as the number of row of the group-IV atom increases. Ge systems have a low-energy transverse acoustic mode along the Γ−M and Γ−K directions. Two transverse acoustic branches along the Γ−A direction are degenerate due to crystal symmetry. Nevertheless, the system under investigation does not show any vibrational anomaly, for example, phonon softening, etc.

Table 2 provides useful data for XA_6 structures: Although clathrate structures XA_6 in Figure 5a depict atomic structures similar to those of A_6, they have different structural parameters showing specific trends. Generally, lattice parameters a and c increase with increasing row number of X = Li, Na, K atoms and A = Si, Ge, Sn atoms. Also, for X = Mg, Ca, the lattice constants increase further. For specific structures, however, d_1 cannot follow the general trend and decreases slightly as a result of energy minimization. Generally, the average cohesive energy E_c displays the reverse trend; namely, it decreases with the increasing row numbers of X and A atoms. Our analysis of atomic charges based on Bader[40] indicates that X atoms donate charge to the metallic bands derived from A atoms. The amount of electronic charge donated by the alkali atoms is −0.7 e and increases with the increasing row number of X. The alkali earth atoms Mg and Ca donate a relatively more electronic charge of −1.2 e, which decreases with the increasing row number of A atoms.

The overall electronic band structures of XA_6 presented in Figure 5c and also in the Supporting Information appear to be essentially similar to those in Figure 3, except for some details. Apart from the changes in the band structures of a XA_6 due to the changes in structural parameters, as well as minute change in the crystal potential of the host A_6, the major change occurs with the dipping of bands relative to the Fermi level or conversely with the raising of the Fermi level due to the electronic charge donated by X atoms. The downward shifts of the bands relative to the Fermi level are even more dramatic in the band structure of X = Mg and Ca, where more electronic charges occur to the increased population of metallic bands and, hence, to the further increase in the Fermi level.

The $ScSi_6$ clathrate system can be stabilized at low and elevated temperatures. The optimized structure, phonon dispersion, and electronic bands of the $ScSi_6$ system are given in Figure S7 (Supporting Information). As seen in Table 2, $ScSi_6$ has the largest cohesion among the systems considered in this work. The distinguished cohesion of Sc in the open hexagonal channels of Si_6 can largely be attributed to the unpaired 3d electron. Generally, XSi_6 clathrates always have larger cohesive energies compared to Ge and Sn clathrates. As a different behavior from other XA_6 clathrates, the contribution of Sc to electronic states at the Fermi level $D(E_F)$ is close to the host Si atoms. The Sc atom donates less electronic charge (1.09 e) to the metallic bands derived from Si compared to $MgSi_6$ and $CaSi_6$. Consequently, the increase in the Fermi level in the $ScSi_6$ clathrate is not as remarkable as $MgSi_6$ and $CaSi_6$ yielding relatively lower $D(E_F)$. On the other hand, it should be noted that the removal of a Sc atom from the $ScSi_6$ clathrate system is rather difficult by thermal processes due to strong binding of the composite system.

CONCLUSIONS

Each group-IV element, namely, C, Si, Ge and Sn, can form a tetrahedrally coordinated cubic diamond structure in their global minimum. The fundamental band gap is as large as 5.4 eV for C, but it diminishes as one goes from C to Sn. In this study, we showed that C, Si, Ge, and Sn can form also elemental clathrate structures, which are metallic with a high state density at the Fermi level. This is a rare situation since group-IV elements construct semiconducting or insulating crystals. Atomic configuration of the clathrate structure is similar for Si, Ge, and Sn and consists of the stacking of atomic planes of nested hexagons with an open channel at the center of the inner hexagon. While the row atoms, which are perpendicular to lateral atomic planes, form 1D metallic chains, the electrons are delocalized in the lateral atomic planes and make 2D metallic states. On the other hand, the atomic configuration of the bare clathrate structure of C is different and can be viewed as hexagonal tubes arranging a 2D hexagonal lattice. Each tube is weakly interacting with its neighbors and the crystal is insulating in the lateral plane, but it

DOI: 10.1021/acs.jpcc.9b03270
J. Phys. Chem. C 2019, 123, 15330−15338

is 1D metallic along the z direction. The interplay of these metallicities in different dimensionalities coexisting in one clathrate structure can give rise to interesting physical effects. By hosting metallic atoms in the open channels, Si, Ge, and Sn can also form stable compound clathrate structures, which are metallic. The host alkali and alkaline earth atoms donate a majority of electronic charge to metallic bands and increase the Fermi level. The open channel can also host hydrogen molecules for storage or can act as a filter for specific atoms. These new allotropes of group-IV elements with their metallic states exhibit features that can be critical fundamentally and technologically.

■ ASSOCIATED CONTENT

Supporting Information

The Supporting Information is available free of charge on the ACS Publications website at DOI: 10.1021/acs.jpcc.9b03270.

Atomic structure, phonons, and electronic structures of compound clathrates of group-IV elements, XA_6 (X = Li, Na, K, Mg, Ca, Sc) (PDF)

■ AUTHOR INFORMATION

Corresponding Authors

*E-mail: ethem.akturk@adu.edu.tr. Phone: +902562130835-1894. Fax: +902562135379 (E.A.).

*E-mail: ciraci@fen.bilkent.edu.tr. Phone: +903122901216. Fax: +903122664579 (S.C.).

ORCID

Fatih Ersan: 0000-0003-0049-105X

Ethem Aktürk: 0000-0002-1615-7841

Notes

The authors declare no competing financial interest.

■ ACKNOWLEDGMENTS

The computational resources are provided by TÜBITAK ULAKBIM, High Performance and Grid Computing Center (TR-Grid e-Infrastructure). This research was supported by the TÜBITAK under project no. 116F059. S.C. acknowledges financial support from the Academy of Sciences of Turkey (TÜBA).

■ REFERENCES

(1) Harrison, W. A. Bond-Orbital Model and the Properties of Tetrahedrally Coordinated Solids. *Phys. Rev. B* **1973**, *8*, 4487.

(2) Choy, M.; Ciraci, S.; Byer, R. Bond-orbital model for second-order susceptibilities. *IEEE J. Quantum Electron.* **1975**, *11*, 40−45.

(3) Harrison, W. A.; Ciraci, S. Bond-orbital model. II. *Phys. Rev. B* **1974**, *10*, 1516−1527.

(4) Durgun, E.; Tongay, S.; Ciraci, S. Silicon and III-V compound nanotubes: Structural and electronic properties. *Phys. Rev. B* **2005**, *72*, No. 075420.

(5) Cahangirov, S.; Topsakal, M.; Aktürk, E.; Şahin, H.; Ciraci, S. Two- and OneDimensional Honeycomb Structures of Silicon and Germanium. *Phys. Rev. Lett.* **2009**, *102*, 236804.

(6) Cahangirov, S.; Özçelik, V. O.; Xian, L.; Avila, J.; Cho, S.; Asensio, M. C.; Ciraci, S.; Rubio, A. Atomic structure of the $\sqrt{3} \times \sqrt{3}$ phase of silicene on Ag(111). *Phys. Rev. B* **2014**, *90*, No. 035448.

(7) Cahangirov, S.; Özçelik, V. O.; Rubio, A.; Ciraci, S. Silicite: The layered allotrope of silicon. *Phys. Rev. B* **2014**, *90*, No. 085426.

(8) Madelung, O. *Semiconductors: Data Handbook*; Springer Science & Business Media, 2012.

(9) Hu, J. Z.; Spain, I. L. Phases of silicon at high pressure. *Solid State Commun.* **1984**, *51*, 263−266.

(10) Duclos, S. J.; Vohra, Y. K.; Ruoff, A. L. Experimental study of the crystal stability and equation of state of Si to 248 GPa. *Phys. Rev. B* **1990**, *41*, 12021.

(11) Minomura, S.; Drickamer, H. G. Pressure induced phase transitions in silicon, germanium and some III−V compounds. *J. Phys. Chem. Solids* **1962**, *23*, 451−456.

(12) Jamieson, J. C. Crystal structures at high pressures of metallic modifications of silicon and germanium. *Science* **1963**, *139*, 762−764.

(13) Wentorf, R. H.; Kasper, J. S. Two new forms of silicon. *Science* **1963**, *139*, 338−339.

(14) Kasper, J. S.; Richards, S. M. The crystal structures of new forms of silicon and germanium. *Acta Crystallogr.* **1964**, *17*, 752−755.

(15) Vohra, Y. K.; Brister, K. E.; Desgreniers, S.; Ruoff, A. L.; Chang, K. J.; Cohen, M. L. Phase-Transition Studies of Germanium to 1.25 Mbar. *Phys. Rev. Lett.* **1986**, *56*, 1944−1947.

(16) Mujica, A.; Rubio, A.; Muñoz, A.; Needs, R. J. High-pressure phases of group-IV, III−V, and II−VI compounds. *Rev. Mod. Phys.* **2003**, *75*, 863.

(17) Crain, J.; Ackland, G. J.; Maclean, J. R.; Piltz, R. O.; Hatton, P. D.; Pawley, G. S. Reversible pressure-induced structural transitions between metastable phases of silicon. *Phys. Rev. B* **1994**, *50*, 13043.

(18) Malone, B. D.; Sau, J. D.; Cohen, M. L. Ab initio survey of the electronic structure of tetrahedrally bonded phases of silicon. *Phys. Rev. B* **2008**, *78*, No. 035210.

(19) Zhao, Y.-X.; Buehler, F.; Sites, J. R.; Spain, I. L. New metastable phases of silicon. *Solid State Commun.* **1986**, *59*, 679−682.

(20) Rapp, L.; Haberl, B.; Pickard, C. J.; Bradby, J. E.; Gamaly, E. G.; Williams, J. S.; Rode, A. V. Experimental evidence of new tetragonal polymorphs of silicon formed through ultrafast laser-induced confined microexplosion. *Nat. Commun.* **2015**, *6*, 7555.

(21) McMahon, M. I.; Nelmes, R. J.; Wright, N. G.; Allan, D. R. Pressure dependence of the Imma phase of silicon. *Phys. Rev. B* **1994**, *50*, 739.

(22) Hanfland, M.; Schwarz, U.; Syassen, K.; Takemura, K. Crystal structure of the highpressure phase silicon VI. *Phys. Rev. Lett.* **1999**, *82*, 1197.

(23) Mylvaganam, K.; Zhang, L. C.; Eyben, P.; Mody, J.; Vandervorst, W. Evolution of metastable phases in silicon during nanoindentation: mechanism analysis and experimental verification. *Nanotechnology* **2009**, *20*, 305705.

(24) Gryko, J.; McMillan, P. F.; Marzke, R. F.; Ramachandran, G. K.; Patton, D.; Deb, S. K.; Sankey, O. F. Low-density framework form of crystalline silicon with a wide optical band gap. *Phys. Rev. B* **2000**, *62*, R7707.

(25) Stefanoski, S.; Malliakas, C. D.; Kanatzidis, M. G.; Nolas, G. S. Synthesis and Structural Characterization of Na_xSi_{136} ($0 < x \leq 24$) Single Crystals and Low-Temperature Transport of Polycrystalline Specimens. *Inorg. Chem.* **2012**, *51*, 8686−8692.

(26) Kurakevych, O. O.; Strobel, T. A.; Kim, D. Y.; Muramatsu, T.; Struzhkin, V. V. Na-Si clathrates are high-pressure phases: A melt-based route to control stoichiometry and properties. *Cryst. Growth Des.* **2013**, *13*, 303−307.

(27) Kim, D. Y.; Stefanoski, S.; Kurakevych, O. O.; Strobel, T. A. Synthesis of an openframework allotrope of silicon. *Nat. Mater.* **2015**, *14*, 169.

(28) Sung, H.-J.; Han, W. H.; Lee, I.-H.; Chang, K. J. Superconducting Open-Framework Allotrope of Silicon at Ambient Pressure. *Phys. Rev. Lett.* **2018**, *120*, 157001.

(29) Lee, J.; Lee, I.-H.; Lee, J. Unbiased Global Optimization of Lennard-Jones Clusters for $N \leq 201$ Using the Conformational Space Annealing Method. *Phys. Rev. Lett.* **2003**, *91*, No. 080201.

(30) Liu, D.; Tománek, D. Effect of Net Charge on the Relative Stability of 2D Boron Allotropes. *Nano Lett.* **2019**, *19*, 1359−1365.

(31) Blöchl, P. E. Projector augmented-wave method. *Phys. Rev. B* **1994**, *50*, 17953.

(32) Kresse, G.; Furthmüller, J. Efficient iterative schemes for ab initio total-energy calculations using a plane-wave basis set. *Phys. Rev. B* **1996**, *54*, 11169.

DOI: 10.1021/acs.jpcc.9b03270
J. Phys. Chem. C 2019, 123, 15330−15338

(33) Kresse, G.; Furthmüller, J. Efficiency of ab-initio total energy calculations for metals and semiconductors using a plane-wave basis set. *Comput. Mater. Sci.* **1996**, *6*, 15−50.
(34) Perdew, J. P.; Burke, K.; Ernzerhof, M. Generalized Gradient Approximation Made Simple. *Phys. Rev. Lett.* **1996**, *77*, 3865.
(35) Grimme, S. Semiempirical GGA-type density functional constructed with a long-range dispersion correction. *J. Comput. Chem.* **2006**, *27*, 1787−1799.
(36) Broyden, C. G. The convergence of a class of double-rank minimization algorithms 1. general considerations. *IMA J. Appl. Math.* **1970**, *6*, 76−90.
(37) Broyden, C. G. The convergence of a class of double-rank minimization algorithms: 2. The new algorithm. *IMA J. Appl. Math.* **1970**, *6*, 222−231.
(38) Methfessel, M.; Paxton, A. T. High-precision sampling for Brillouin-zone integration in metals. *Phys. Rev. B* **1989**, *40*, 3616.
(39) Monkhorst, H. J.; Pack, J. D. *Phys. Rev. B* **1976**, *13*, 5188.
(40) Henkelman, G.; Arnaldsson, A.; Jónsson, H. A fast and robust algorithm for Bader decomposition of charge density. *Comput. Mater. Sci.* **2006**, *36*, 354−360.
(41) Baroni, S.; de Gironcoli, S.; Dal Corso, A.; Giannozzi, P. Phonons and related crystal properties from density-functional perturbation theory. *Rev. Mod. Phys.* **2001**, *73*, 515−562.
(42) Togo, A.; Tanaka, I. First principles phonon calculations in materials science. *Scr. Mater.* **2015**, *108*, 1−5.
(43) Momma, K.; Izumi, F. VESTA 3 for three-dimensional visualization of crystal, volumetric and morphology data. *J. Appl. Crystallogr.* **2011**, *44*, 1272−1276.
(44) Vogt, P.; De Padova, P.; Quaresima, C.; Avila, J.; Frantzeskakis, E.; Asensio, M. C.; Resta, A.; Ealet, B.; Le Lay, G. Silicene: Compelling Experimental Evidence for Graphenelike Two-Dimensional Silicon. *Phys. Rev. Lett.* **2012**, *108*, 155501.

DOI: 10.1021/acs.jpcc.9b03270
J. Phys. Chem. C 2019, 123, 15330−15338